

Efficient estimation of rare-event kinetics

Benjamin Trendelkamp-Schroer* and Frank Noé†

Institut für Mathematik und Informatik, FU Berlin, Arnimallee 6, 14195 Berlin

(Dated: October 15, 2018)

The efficient calculation of rare-event kinetics in complex dynamical systems, such as the rate and pathways of ligand dissociation from a protein, is a generally unsolved problem. Markov state models can systematically integrate ensembles of short simulations and thus effectively parallelize the computational effort, but the rare events of interest still need to be spontaneously sampled in the data. Enhanced sampling approaches, such as parallel tempering or umbrella sampling, can accelerate the computation of equilibrium expectations massively - but sacrifice the ability to compute dynamical expectations. In this work we establish a principle to combine knowledge of the equilibrium distribution with kinetics from fast “downhill” relaxation trajectories using reversible Markov models. This approach is general as it does not invoke any specific dynamical model, and can provide accurate estimates of the rare event kinetics. Large gains in sampling efficiency can be achieved whenever one direction of the process occurs more rapid than its reverse, making the approach especially attractive for downhill processes such as folding and binding in biomolecules.

I. INTRODUCTION

A wide range of biological or physico-chemical systems exhibit rare-event kinetics, consisting of rare-transitions between a couple of long-lived (meta-stable) states. Examples are protein-folding, protein ligand association, and nucleation processes. Meta-stability can be found in any system in which states of minimum energy are separated by barriers higher than the average thermal energy.

A thorough understanding of such systems encompasses the kinetics of the rare-events, e.g. rates and transition pathways. Obtaining reliable estimates for such systems is notoriously difficult: The simulation time needs to exceed the longest waiting time, resulting in a sampling problem.

In recent years, Markov state models (MSMs) [1–8] and their practical applicability through software [9, 10] have become a key technology for computing kinetics of complex rare-event systems. A well-constructed MSM separates the kinetically distinct states and captures their transition rates or probabilities. With a suitable choice of state space discretization and lag-time, kinetics can be approximated with high numerical accuracy [8, 11]. MSMs can be straightforwardly interpreted and analyzed with Markov chain theory and Transition Path Theory [12, 13]. This was demonstrated, for example, for protein folding [14, 15] or protein-ligand binding [16, 17].

MSMs can somewhat alleviate the sampling problem by virtue of the fact that they can be estimated from short simulations produced in parallel [14, 15, 18], thus avoiding the need for single long trajectories [19]. However, the rare-events of interest must be sampled in the data in order to be captured by the model. For example, in protein-ligand binding, a dissociation rate can only be

computed if each step of the dissociation process has been sampled at least once.

Orders of magnitude of speedup can be achieved with enhanced sampling methods such as umbrella sampling, replica exchange dynamics, or meta-dynamics [20–23]. The speedup is achieved by coupling the unbiased ensemble of interest with ensembles at higher temperature at which the rare-events occur more frequently or by using biasing potentials allowing to “drag” the system across an energy barrier. With such approaches, accurate equilibrium expectations, such as free energy profiles can be computed efficiently, but the dynamical properties of the unbiased ensemble, such as transition rates, relaxation time-scales and transition pathways, are generally not available.

A common approach to reconstruct the kinetics from the free energy profiles is to employ rate theories such as transition state theory, Kramer’s or Smoluchowski/Langevin models [24–27]. Such dynamical models introduce additional assumptions that cannot be self-consistently validated because the predicted dynamics is not present in the data.

A much more advanced approach was recently introduced in [28], where an MSM-based estimator for the stationary vector using transition counts harvested from simulations at different thermodynamic states, such as umbrella sampling. This approach allows to mix, in principle, umbrella sampling simulations and direct molecular dynamics and compute the rates from the transition matrix of the unbiased ensemble. However, the coefficient matrices used to connect the biased and unbiased transition matrices require a specific dynamical model to be formulated (such as Brownian dynamics in the free energy coordinate), making this approach essentially a rate model. In general, key assumptions underlying rate models are usually the existence of a time-scale separation and approximate Markovianity on a single or few reaction coordinates - assumptions that are unlikely to hold for complex multi-state systems describing, e.g. biomolecular dynamics.

* benjamin.trendelkamp-schroer@fu-berlin.de

† frank.noé@fu-berlin.de; “corresponding author”

The recently introduced transition-based reweighting analysis methods (TRAM) [29–31] permit to rigorously combine direct molecular dynamics and enhanced sampling methods towards full thermodynamics and kinetics without assuming any restrictive rate model. However, a current limitation is that in order to extract unbiased kinetics, the transition events need to be evaluated at a common and sufficiently large lag time τ at all thermodynamic states. This requirement is not consistent with efficient umbrella sampling or replica-exchange MD simulations that typically employ very short simulation snippets.

Finally, computation of kinetic quantities without rate models is also possible with path sampling methods, such as transition path sampling [32], milestoning [33], transition interface sampling [34], and multi-state transition interface sampling [35]. A challenge is that these approaches are essentially two-state methods. The transition end-states must be defined a-priori and all relevant rare-events must be distinguishable in the reaction coordinates, cores, or milestones that the method operates on.

Here we construct a general simulation approach that enables the computation of kinetic observables related to slow processes without having to explicitly sample the rare-events. It is based upon a very simple but general idea: Simulations are often constructed in such a way that they obey microscopic reversibility or at least a generalization thereof [36, 37]. In this case, for any partition of state space into sets i, j, \dots and any choice of the lag-time τ , we have the detailed balance relation

$$\pi_i p_{ij}(\tau) = \pi_j p_{ji}(\tau), \quad (1)$$

where $p_{ij}(\tau)$ is the probability of making a transition from set i to set j within a time τ and π_i is the equilibrium probability of set i . Suppose we have knowledge about the equilibrium probabilities π_i, π_j from an enhanced sampling simulation. Then only the larger one of the two transition probabilities - p_{ij} or p_{ji} - needs to be sampled while the less probable event can be reconstructed by (1).

Speaking in terms of a network of states, a direct analysis or an analysis via Markov state models requires all states to be connected in both directions (strongly connected). The presented method allows to relax this requirement if an estimate of the equilibrium probabilities is given - now all states need to be only connected in one direction (weakly connected).

The slow rate exhibits a functional dependence on the transition probabilities of the slow event. By virtue of the detailed balance condition a reliable estimate of the transition probabilities for the frequent event entails a reliable estimate for the transition probabilities of the slow event - resulting in a reliable estimate of the slow rate.

While the inference procedure is trivial for a two-state system where three of the four components in (1) are known exactly, it is far from trivial for a system with

many states and when some or all estimates are subject to statistical uncertainty. Here we establish a systematic inference scheme for combining multi-state estimates of the equilibrium probabilities (π_i) with sampling data of at least the “down-hill” transition probabilities p_{ij} . Our approach is built upon the framework of reversible Markov models [38, 39] where (1) is enforced between all pairs of states. As a consequence, our estimates do not invoke any additional dynamical model, are accurate within a suitable state space discretization [8, 11], and are precise in the limit of sufficient sampling.

In contrast to the DHAM and TRAM methods we use the stationary probabilities already estimated from enhanced sampling simulation as additional input parameters for the estimation of MSM transition probabilities. Standard reweighting schemes used to obtain the stationary probabilities do usually not assume a dynamical model to obtain the desired unbiased probabilities.

The estimation procedure can reduce the sampling problem tremendously for processes with some long-lived states and some other states from which the system relaxes rapidly. This case is ubiquitous in meta-stable systems, because long-lived states are connected by short-lived transition states. But even long-lived states usually have very different lifetimes: For example many ligands or inhibitors bind to their protein receptor with nanomolar concentrations, meaning that the transition probabilities leading to the associated state are orders of magnitude higher than the dissociation probabilities. The present reversible Markov model approach lays the basis for estimating the kinetics and mechanisms of protein-drug dissociation by combining the much more rapid association trajectories with suitable enhanced sampling methods such as Hamiltonian replica-exchange [40] or umbrella sampling [18, 41].

II. THEORY

A. Markov state models

Classical dynamics, governed by Newton’s equations in the case of an isolated system and by Langevin equation’s for systems at constant temperature [42], gives rise to a transfer operator \mathcal{P} propagating a phase-space density from time t to time $t + \Delta t$ [43–45]. Numerical solutions for Newton’s or Langevin equations can be obtained for complex systems with many degrees of freedom, but a direct numerical assessment of the transfer operator is in most cases prohibited due to the curse of dimensionality.

Markov state models (MSMs) bridge this gap estimating the transfer operator on a suitably defined state space partition

$$\Omega = \{s_1, \dots, s_n\}. \quad (2)$$

using trajectories obtained by direct numerical simulation [8, 11].

MSMs model the jump process between states of this partition by a Markov chain. Observed transitions between pairs of states i and j are collected in a *count matrix* $C = (c_{ij})$ and the likelihood for the observed counts for a given *transition matrix* $P = (p_{ij})$ is given by

$$\mathbb{P}(C|P) \propto \prod_i \left(\prod_j p_{ij}^{c_{ij}} \right). \quad (3)$$

While the likelihood functions allows to determine the maximum likelihood estimator \hat{P} optimizing the likelihood function for a given observation C over the set of all possible models P it does not specify the uncertainty of a chosen model.

For a finite amount of observation data there will in general be a whole ensemble of models compatible with the given data. In order to specify uncertainties and determine statistical errors of estimated quantities we need to infer the posterior probability of a model for a given observation. An application of Bayes' formula yields

$$\underbrace{\mathbb{P}(P|C)}_{\text{posterior}} \propto \underbrace{\mathbb{P}(P)}_{\text{prior}} \underbrace{\mathbb{P}(C|P)}_{\text{likelihood}}. \quad (4)$$

For a uniform prior, i.e. no a priori knowledge about the model, the posterior probability is given as a product of *Dirichlet distributions*

$$\mathbb{P}(P|C) \propto \prod_i \left(\prod_j p_{ij}^{c_{ij}} \right). \quad (5)$$

B. Inference using a given stationary vector

There are many methods that allow to efficiently estimate the stationary vector, even in situations in which a direct estimation from a finite observation of the Markov chain is unfeasible due to the meta-stable nature of the system [20–23, 46, 47]. In such situations it is often possible to alter the system dynamics in a controlled way such that the artificial dynamics equilibrates more rapidly than the original one. The desired stationary vector of the original dynamics can then be related to the stationary vector estimated from the altered process [48–52].

In the following we want to show how such prior knowledge about the stationary vector can be used to improve the estimates of kinetic observables in systems with rare-events.

We are again given a finite observation of a Markov chain in terms of the count matrix C . Assume we are additionally given the stationary vector π for our system of interest and we know that the transition probabilities of the chain fulfil detailed balance for the given stationary vector,

$$\pi_i p_{ij} = \pi_j p_{ji}. \quad (6)$$

Then we can express the posterior probability for our model via (4). Prior knowledge about the stationary vector π in combination with the detailed balance assumption formally entails the following prior distribution on the posterior ensemble,

$$\mathbb{P}(P|\pi) = \prod_{i < j} \delta(\pi_i p_{ij} - \pi_j p_{ji}). \quad (7)$$

According to (4) the constrained posterior is

$$\mathbb{P}(P|C, \pi) \propto \mathbb{P}(P|\pi) \mathbb{P}(C|P). \quad (8)$$

The effect of the prior (7) is a restriction of the posterior to the subspace of transition matrices fulfilling detailed balance with respect to the fixed stationary vector π .

C. Maximum likelihood estimate given a stationary vector

We can also use prior knowledge of the stationary vector to constrain the maximum likelihood estimate \hat{P} to the set of matrices obeying (6) for a given stationary vector π . This results in the following convex constrained optimization problem

$$\begin{aligned} &\text{minimize} && - \sum_{i,j} c_{ij} \log p_{ij} \\ &\text{subject to} && p_{ij} \geq 0 \\ &&& \sum_j p_{ij} = 1 \\ &&& \pi_i p_{ij} = \pi_j p_{ji} \end{aligned} \quad (9)$$

which can be solved using methods outlined in [53].

D. Inference using a stationary vector with uncertainty

A stationary vector estimate usually carries a finite sampling error which should be accounted for when inferring a reversible transition matrix from data. From a Bayesian viewpoint we have to combine two sources of evidence. The observed count-matrix C from standard equilibrium simulations and the data from enhanced or biased sampling methods E used to estimate the stationary vector.

An error model for the estimation of uncertainty in the stationary vector assess the posterior of stationary vectors given the enhanced sampling data, $\mathbb{P}(\pi|E)$. Recent methods for the uncertainty quantification of reversible MSMs with fixed stationary vector allow to sample the posterior $\mathbb{P}(P|\pi, C)$ in (8).

The posterior for transition matrices under the combined evidence $\mathbb{P}(P|C, E)$ can be formally decomposed as

$$\mathbb{P}(P|C, E) = \int d\pi \mathbb{P}(P|C, \pi, E) \mathbb{P}(\pi|C, E). \quad (10)$$

Assuming that the direct effect of the enhanced sampling information E is negligible in the posterior of transition matrices with given stationary vector,

$$\mathbb{P}(P|C, \pi, E) \approx \mathbb{P}(P|C, \pi) \quad (11)$$

and that the direct effect of observed transition counts C is unimportant compared to the enhanced sampling data used to obtain π from a standard reweighting scheme,

$$\mathbb{P}(\pi|C, E) \approx \mathbb{P}(\pi|E) \quad (12)$$

we model the uncertainty encoded in the desired posterior by inserting the two approximations (11), (12) into (10)

$$\mathbb{P}(P|C, E) \approx \int d\pi \mathbb{P}(P|C, \pi) \mathbb{P}(\pi|E). \quad (13)$$

Approximate sampling from $\mathbb{P}(P|C, E)$ can now be achieved by drawing a random sample $\pi^{(1)}, \dots, \pi^{(M)}$ distributed according to a given error-model, $\pi^{(k)} \sim \mathbb{P}(\pi|E)$ and generating a sample of transition matrices $P_1^{(k)}, \dots, P_N^{(k)}$ from the constrained posterior $P_i^{(k)} \sim \mathbb{P}(P|C, \pi^{(k)})$ for each of the $\pi^{(k)}$. The sample $P_1^{(1)}, \dots, P_N^{(1)}, \dots, P_1^{(M)}, \dots, P_N^{(M)}$ will then be approximately distributed according to $\mathbb{P}(P|C, E)$.

In [39] we have presented a Markov chain Monte Carlo approach to sample reversible transition matrices fulfilling detailed balance with respect to a fixed stationary vector. This method however has suffered from poor acceptance probabilities. In [53] we outline a method to efficiently generate samples from the constrained posterior using a Gibbs sampling algorithm that will be used here.

For given vector (π_i) detailed balance (6) enforces a linear dependence between the transition matrix element p_{ij} and the element p_{ji} . As an immediate consequence the standard error of both elements for a sample generated from the posterior $\mathbb{P}(P|C)$ has to be equal,

$$\frac{\sqrt{\mathbb{V}(p_{ji})}}{\mathbb{E}(p_{ji})} = \frac{\sqrt{\mathbb{V}(p_{ij})}}{\mathbb{E}(p_{ij})}. \quad (14)$$

We will show how this can be used in order to significantly improve various estimates in situations in which $p_{ij} \ll p_{ji}$.

III. RESULTS

In the following we will demonstrate the usefulness of (14) via a comparison of the standard error for kinetic quantities depending on rare-events that are either estimated from a Markov model of the direct unbiased simulation (unconstrained posterior (5)), as well as when enhanced sampling data is additionally used (constrained posterior (8) or constrained posterior with uncertain stationary vector (13)).

A. Finite state space Markov chain

Consider a three-state Markov chain with the following transition matrix

$$P = \begin{pmatrix} 1 - 10^{-b} & 10^{-b} & 0 \\ \frac{1}{2} & 0 & \frac{1}{2} \\ 0 & 10^{-b} & 1 - 10^{-b} \end{pmatrix}. \quad (15)$$

The parameter $b > 0$ can be thought of as the height of an energy barrier between states one and three. The corresponding stationary distribution is given by

$$\pi = (1 + 10^{-b})^{-1} \left(\frac{1}{2}, 10^{-b}, \frac{1}{2} \right)^T. \quad (16)$$

The pair (π, P) satisfies the detailed balance equation (6).

Any process starting in state one has an exponential small probability of crossing over to state three. In fact a chain starting in state one can reach state three only via state two, but the probability to go from state one to state two is exponentially small in the barrier height b . The reversed process, going from state two to state one, occurs much faster. The same applies to state three and state two. The eigenvalues of this matrix are

$$\lambda_1 = 1 \quad \lambda_2 = 1 - 10^{-b} \quad \lambda_3 = -10^{-b}.$$

and the slowest time-scale in the system is given by,

$$t_2 = -\frac{1}{\log \lambda_2} \approx 10^b.$$

It is apparent from $t_2 \approx p_{12}^{-1}$ that estimates of t_2 and of p_{12} have similar standard errors. The standard error ϵ for a matrix-element p_{ij} for sampling from the unconstrained posterior (5) is

$$\epsilon(p_{ij}) = \frac{1}{\sqrt{c_{ij}}}.$$

For $b = 4$ and a single chain of length $N \approx 7 \cdot 10^4$ steps starting in state one we can on average expect $c_{12} = 4$ resulting in a relative standard error of 50%. In order to decrease the error down to 1% we would need to run a chain of length $N \approx 100^2 \cdot 10^4 = 10^8$ steps. This is clearly an unsatisfactory situation and we would like to reduce the required simulation effort to reach a given error level as much as possible.

In comparison for an ensemble of M short chains of length L , with $L \ll 10^b$, starting in state two one will on average observe a transition from state two to state one for every second chain, $c_{21} = M/2$, so that a relative error of 1% for p_{21} can already be achieved for $M \approx 10^4$, with $L \ll 10^b$, so that the total simulation effort can be reduced by orders of magnitude.

We do not have explicit expressions for the standard error of matrix elements p_{ij} when sampling from the restricted ensemble enforcing detailed balance with respect

to a given stationary vector. It is however conceivable that the standard errors of p_{21} can be reduced in the same way. The relation (14) guarantees that a small error for p_{21} will also result in a small error for the rare-event quantity p_{12} .

Figure 1 shows the standard error of t_2 versus the total simulation effort. The error for a single long chain is estimated from a sample of transition matrices generated from the unconstrained posterior. The error for the ensemble of short chains is estimated from a sample of transition matrices generated from the constrained posterior using the algorithm outlined in [53]. From Figure 1 it is apparent that using a-priori information about the stationary vector in combination with an ensemble of short simulations started from the unstable state results in a three orders of magnitude smaller simulation effort when trying to estimate t_2 with a prescribed error. In particular, estimation of the rare-event kinetics can be conducted orders of magnitude before a direct simulation would even encounter a single transition event.

This effect is even more pronounced when choosing $b = 9$ so that estimation via long trajectories sampling the rare event is hopeless. Using short trajectories starting in the transition state in combination with the stationary vector one can accurately estimate t_2 with a total simulation effort of $N = 10^3$ steps, c.f. Figure 2. That is six orders of magnitude before on average even a single rare-event would have been observed.

B. Double-well potential

Let us now go to an example where the Markov state model is an approximation of the true dynamics. We employ Brownian dynamics in a double-well potential defined by

$$V(x) = (x^2 - \sigma^2)^2 + \delta\sigma\left(\frac{1}{3}x^3 - \sigma^2x\right). \quad (17)$$

The two minima of the potential at $\pm\sigma$ are separated by a maximum at $-\delta\sigma/4$, cf. Figure 3. The dynamics is governed by the following SDE,

$$dX_t = -\nabla V(X_t) + \sqrt{2\beta^{-1}}dW_t, \quad (18)$$

with dW_t denoting the increments of the *Wiener-process*. The inverse temperature $\beta = (k_B T)^{-1}$ controls the intensity of the stochastic fluctuations.

(18) defines a process where X_t sample from the canonical distribution,

$$\pi(x) = Z(\beta)^{-1}e^{-\beta V(x)}. \quad (19)$$

The temperature dependent constant $Z(\beta)$ is the *partition function* ensuring correct normalization, $\int dx \pi(x) = 1$. Spectral properties of this Markov process, such as the largest implied time-scale can be computed from a spatial discretisation of its associated transition kernel, cf. section A.

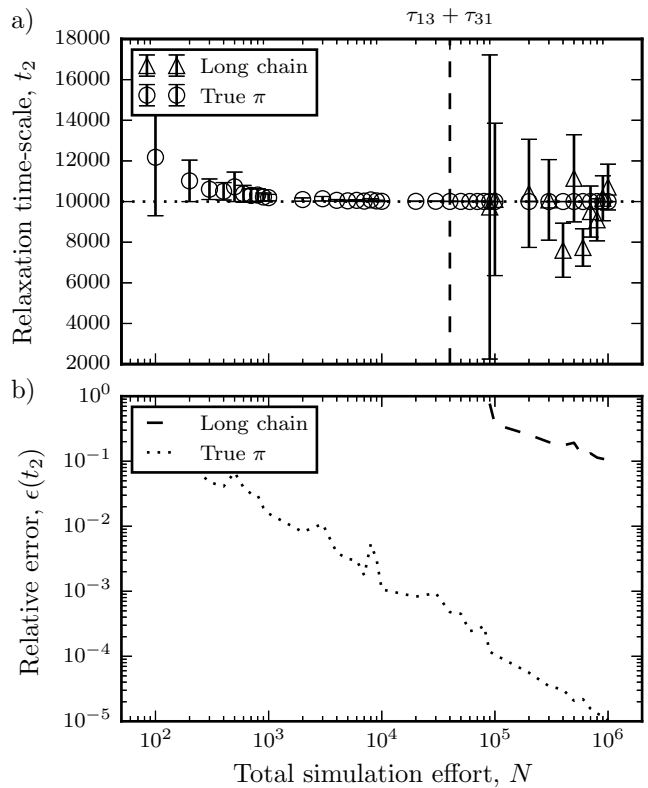


Figure 1. Mean and standard error of the largest implied time-scale t_2 , total simulation effort N for meta-stable 3-state system with barrier parameter $b = 4$. a) Convergence of the mean value, using either a single long trajectory starting in one of the meta-stable states or the stationary vector together with an ensemble of short chains relaxing from the transition state. The latter approach allows to obtain a reliable estimate already before the average waiting time for a single rare-event $\tau_{13} + \tau_{31}$ has elapsed. The comparison of the estimated standard error b) indicates a three orders of magnitude speedup when estimating the rare-event sensitive quantity t_2 using the stationary vector in combination with short relaxation trajectories.

For the numerical experiment we used a double-well potential with parameters $\sigma = 2.2$ and $\delta = 0.1$. The time step for the explicit Euler-scheme is $\Delta t = 10^{-3}$. The noise parameter is $\beta = 0.4$.

Spatial discretization of the transition kernel is performed with $L_x = 3.4$ and $n_x = 400$ regular sub-intervals. The matrix (p_{ij}) is assembled by evaluating the kernel at the midpoints of the sub-intervals. The largest implied time scale, $t_2 = 1.2 \cdot 10^6$, is computed from an eigenvalue decomposition of the assembled matrix. Mean first passage times between sets $A = [\sigma - 0.2, \sigma + 0.2]$ and $B = [-\sigma - 0.2, -\sigma + 0.2]$ are computed as $\tau_{AB} = 5.3 \cdot 10^6$ and $\tau_{BA} = 1.6 \cdot 10^6$, see section B for details. Values computed from the spatial discretization are used as reference values for comparison with estimates obtained from a Markov model.

The Markov model is build using a regular grid dis-

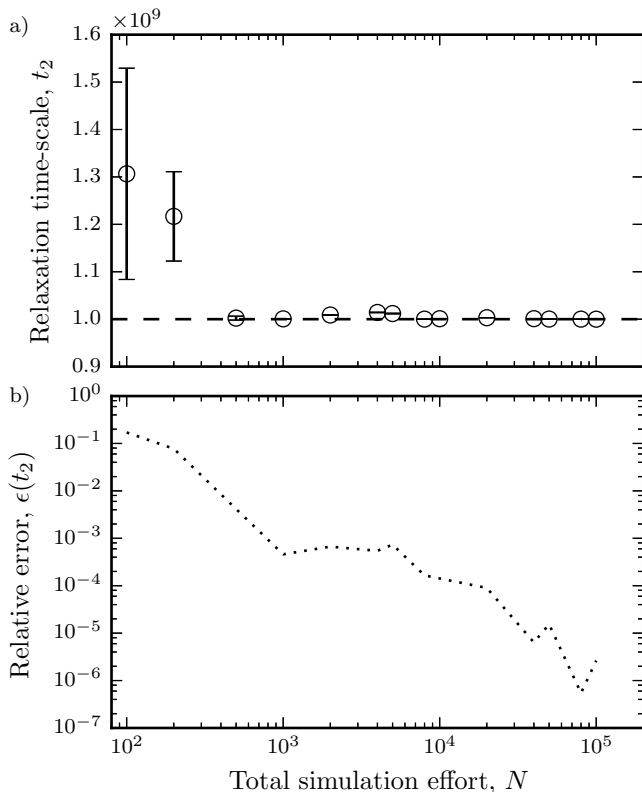


Figure 2. Mean and standard error of the largest relaxation time-scale, t_2 , total simulation effort N for meta-stable 3-state system with barrier parameter $b = 9$. a) Convergence of the mean value using short trajectories relaxing from the transition state. A correct estimate can be obtained six orders of magnitude before a single rare-event would have occurred on average. b) Standard error of the estimate. The estimation using long trajectories is unfeasible.

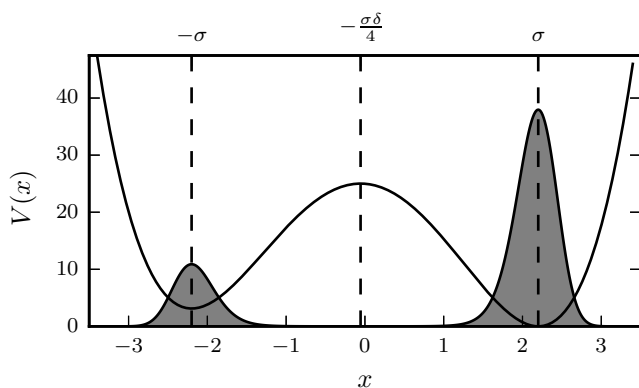


Figure 3. Potential $V(x)$ and stationary distribution $\pi(x)$, for Brownian dynamics in double-well potential. The stationary distribution (shaded area) is scaled to fit the scale of the potential function. It can be seen that the stationary probability is concentrated in the meta-stable regions around the two minima of the potential at $\pm\sigma$.

cretization of $[-L, L]$ with $L = 3.4$ and $n = 100$ states. From an implied time scale estimation using long trajectories with $N = 10^8$ steps we obtain a lag-time of $\tau = 10 dt$.

The stationary vector is estimated from umbrella sampling simulations using the weighted histogram analysis method [49, 54]. Estimates were computed using $M_\pi = 20$ umbrella sampling simulations with $L_\pi = 2.5 \cdot 10^4$ points per umbrella as well as from umbrella sampling simulations with $L_\pi = 5 \cdot 10^6$ points per umbrella. To account for the uncertainty in the estimated stationary vector we used bootstrap resampling [55] of the generated data and computed the stationary distribution for each re-sampled data set to model the ensemble of stationary vectors compatible with the observed umbrella sampling data.

In Figure 4 we show mean and standard error of the largest implied time scale t_2 versus the total simulation effort N . The total simulation effort N is composed of the simulation effort spent on obtaining a count matrix from standard simulations, N_C , and the simulation effort spent on obtaining the stationary distribution from umbrella sampling simulations, N_π ,

$$N = N_\pi + N_C. \quad (20)$$

We compare three different approaches when estimating mean and standard error of the largest implied time-scale t_2 .

1. Generate a single trajectory starting in one of the meta-stable regions and compute estimates without a priori knowledge of the stationary vector.
2. Generate an ensemble of short trajectories starting on the barrier and compute estimates with an error-model for the stationary vector as prior information.
3. Balanced sampling: split the total simulation effort equally between umbrella simulations and short trajectories starting on the barrier, $N_\pi = N_C = N/2$. Compute estimates updating the error model for the stationary vector according to the increasing amount of data available for the estimation.

Transition matrices are sampled according to (5) if no prior knowledge about the stationary vector is available and from (13) if the stationary vector was estimated from umbrella simulation data. For the first approach we use $M_C = 20 \dots 100$ long trajectories of length $L_C = 10^6 dt$ starting in the minimum point, $x_0 = s$, and for the second approach we use an ensemble of $M_C = 50 \dots 5000$ short trajectories of length $L_C = 10^4 dt$ starting on the barrier, $x_0 = -\delta\sigma/4$. For the second approach we have estimated the stationary vector from a small as well as for a large amount of umbrella sampling data in order to demonstrate the dependence of the standard error of the kinetic observable on the error in the ensemble of input stationary distributions.

It can be seen from Figure 4 that for a fixed effort $N_\pi = M_\pi L_\pi$ the standard error can not be reduced below a certain amount with increasing $N_C = M_C L_C$. This is a result of the non-zero statistical error in the estimate of the stationary vector for fixed N_π . The usual $N^{-\frac{1}{2}}$ dependence of the standard error can be recovered for the proposed splitting $N_\pi = N_C = N/2$. Figure 4 shows the favourable scaling coefficient of such an approach leading to a more than two orders of magnitude faster convergence of the estimated quantity compared to using standard simulations alone. Reliable estimates of the rare-event kinetics can be obtained one order of magnitude simulation effort before the standard approach using long trajectories and no information about the equilibrium probabilities can be applied at all. The finite error for the estimate of the stationary vector for $N_\pi = 5 \cdot 10^4 dt$ and $N_\pi = 10^7 dt$ results in a saturation of the error of t_2 which can be further decreased using a more precise estimate of the stationary vector from additional enhanced sampling simulations.

For metastable systems we propose the following strategy for distributing initial conditions exploiting the information from the equilibrium vector. Once all metastable sets and all kinetic barriers separating the sets have been identified using some enhanced sampling protocol, short trajectories should be started on top of all barriers or in high-energy metastable states. The length of the short trajectories needs to be sufficient to relax towards the low-energy metastable states. The method described here can be used to combine these data to an estimate of the full rare-event kinetics.

C. Alanine dipeptide

As an example for a rare-event quantity in a molecular system we use the mean first-passage time for the C_5 to C_7^{ax} transition in the alanine-dipeptide molecule. Alanine-dipeptide has been the long-serving laboratory rat of molecular dynamics [56–60]. The ϕ and ψ dihedral angles have been identified as the two relevant coordinates for the slowest kinetic processes of the system in equilibrium. The potential of mean force for the two dihedral angles is shown in Figure 5.

One can identify five meta-stable regions in the free-energy landscape. The C_5 and P_{II} regions correspond to dihedral angles found in a beta-sheet conformation, the α_R and α_L regions correspond to a right, respectively left-handed α -helix conformation. Reference values for the mean-first passage times between all pairs of sets have been computed from the maximum likelihood estimator of (3) using a total of $10\mu s$ of simulation data. Values can be found in Table I. For details of the computation of mean first-passage times see section B.

All computations were carried out on high-performance GPU cards using the OpenMM simulation package [61]. The used forcefield was *amber99sb-ildn* [62] and the used water-model was *tip3p* [63]. The

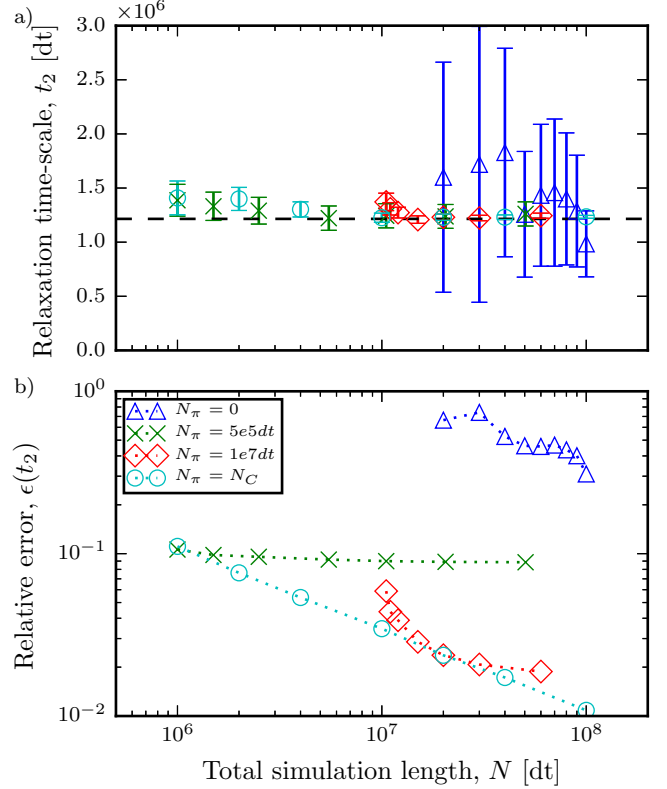


Figure 4. Mean and standard error of largest implied time-scale t_2 , given total simulation effort N , for Brownian dynamics in double-well potential. a) Convergence of the mean value, using either a single long trajectory starting in one of the meta-stable states or the stationary vector together with an ensemble of short chains relaxing from the transition state. The latter approach allows to obtain a reliable estimate already before the average waiting time for a single rare-event $\tau_{AB} + \tau_{BA}$ has elapsed. A comparison of the standard error b) indicates a more than two orders of magnitude speedup when estimating the rare-event sensitive quantity t_2 . By combining short trajectories with information about the stationary probabilities, reliable estimates of the slowest relaxation timescale can be obtained with a total amount of simulation data that is about one order of magnitude smaller than the expected waiting time for a forward and backward transition across the barrier.

τ_{AB}/ns	C_5	P_{II}	α_R	α_L	C_7^{ax}
C_5	0	0.021	0.253	43.456	60.220
P_{II}	0.041	0	0.255	43.449	60.213
α_R	0.142	0.125	0	43.549	60.312
α_L	1.553	1.527	1.744	0	17.757
C_7^{ax}	1.559	1.533	1.745	1.221	0

Table I. Mean first passage time (mfpt) between meta-stable regions of alanine-dipeptide. The mfpts have been estimated from $10\mu s$ of simulation data using a Markov state model.

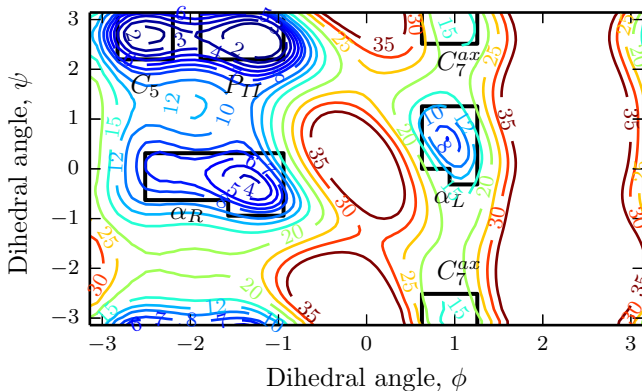


Figure 5. Free energy profile of alanine-dipeptide as a function of the dihedral angles. Energies are given in kJ/mol . The average thermal energy $k_B T$ at 300K is 2.493kJ/mol . One can identify five meta-stable sets on the dihedral angle torus, here indicated by black lines. There are three low energy (high probability) sets C_5 , P_{II} and α_R with $\phi < 0$ and two high energy (low probability) sets α_L and C_7^{ax} with $\phi > 0$.

peptide was simulated in a cubic box of 2.7nm length including 652 solvent molecules. Langevin equations were integrated at $T = 300\text{K}$ using a time-step dt of 2fs . The potential used for umbrella sampling simulations was $V_i(\phi) = k[1 + \cos(\phi - \phi_i - \pi)]$ with $k = 200\text{kJ/mol}$. Umbrellas were placed at a spacing of $\phi_i - \phi_{i+1} = 9^\circ$.

1. Analysis in ϕ and ψ dihedral angle space

We show the convergence of the largest relaxation timescale and validate the MSM constructed at a lagtime of $\tau = 6\text{ps}$ via a Chapman-Kolmogorov test in Figure 12. Convergence of the largest relaxation time indicates that the slow eigenfunctions of the associated dynamical operator are well approximated by the discrete MSM. The Chapman-Kolmogorov-test explicitly checks the Markov assumption comparing self transition probabilities computed from the MSM, parametrized at lagtime τ , with direct estimates from the data at larger lagtimes, $n\tau$. A thorough discussion of MSM validation can be found in [8].

In Figure 6 we show the estimate of the mean first-passage time τ_{AB} between the C_5 and the α_L region together with the corresponding standard error $\epsilon(\tau_{AB})$ for different values of the total simulation effort N . The simulation setup is similar to the one described for the double-well potential in the previous section. Instead of starting short trajectories directly on the barrier we start them from the meta-stable α_L region. Figure 6 shows that combining umbrella sampling data and short trajectories relaxing from a meta-stable region with low probability (high free-energy) towards a meta-stable state with high probability (low free-energy) is able to estimate the reference value, $\tau_{AB} = 43\text{ns}$ for the C_5 to α_L transition

with a total simulation effort of 70ns if short ‘downhill’ trajectories are used in combination with umbrella sampling data. Utilizing information about the equilibrium distribution in combination with short simulations that do not have to sample the rare event is able to achieve a standard error with almost an order of magnitude less simulation effort compared to an ensemble of long trajectories. The observed 8-fold speedup is in good agreement with the expected speedup given by

$$\frac{\tau_{AB}}{L}$$

with $\tau_{AB} = 43\text{ns}$ the mfpt for the slow “up-hill” transition from C_5 to α_L , and $L = 5\text{ns}$ the length of individual short trajectories.

The present approach of estimating rare-event kinetics is more powerful than traditional rate theories because quantities that can be estimated can be much more complex than only rates. As a reversible Markov model is estimated, full mechanisms, such as the ensemble of transition pathways from one state to another state can be computed. To illustrate this we compute the committor probability function, cf. section C, from C_5 to α_L using both estimates. It is seen that information about the stationary vector results in nearly the same committor function as one estimated using an order of magnitude larger simulation effort.

2. Analysis in the ϕ -coordinate alone

The presented method can also work if only information about the slowest degree of freedom is used. In Figure 8 we show the free energy profile for the ϕ dihedral angle. An energetic barrier clearly separates the low free energy region, $\phi < 0$ from the high free energy region, $\phi > 0$. Crossing events from $\phi < 0$ to $\phi > 0$ are rare leading to a sampling problem if kinetic quantities associated with barrier-crossings need to be estimated. Again we show convergence of the largest relaxation time-scale, t_2 and a Chapman-Kolmogorov test for a MSM estimated at lagtime $\tau = 15\text{ps}$, Figure 13.

In Figure 9 we show that the correct mean first passage time for the C_5 to α_L transition can also be recovered from the MSM of the ϕ angle alone. This demonstrates that the presented method is robust with respect to the choice of microstates. Choosing a slightly larger lagtime $\tau = 15\text{ps}$ for the ϕ MSM allowed to recover the correct mean first passage times despite the fact that information about the ψ dihedral angle was completely neglected. The MSM for ϕ dihedral angle is still a good approximation to the true kinetics if the discretization and the lagtime are suitably matched. A thorough discussion of approximation errors for MSMs can be found in [8, 11].

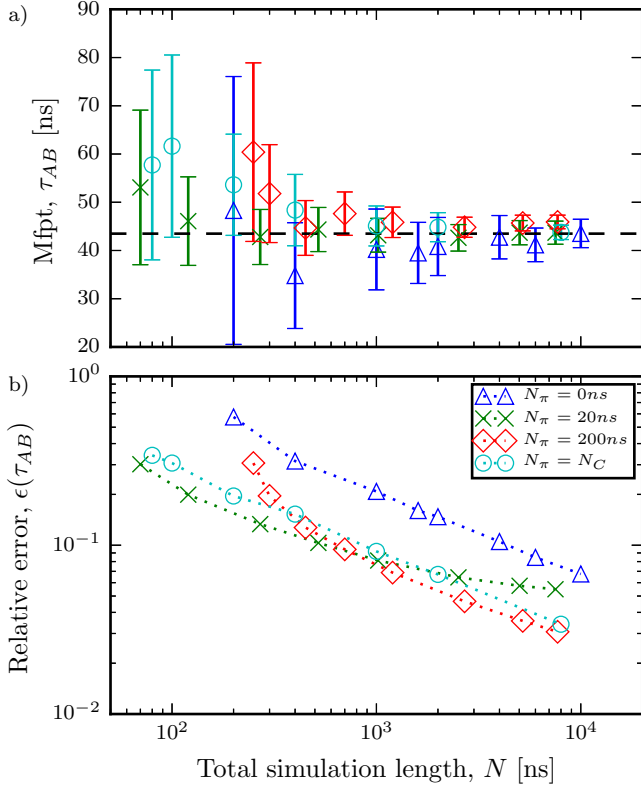


Figure 6. Mean and standard error of mean first passage time (mfpt) τ_{AB} , total simulation effort N , for alanine-dipeptide MSM on the ϕ, ψ dihedral angles. The mean first-passage time τ_{AB} of the C_5 to α_L transition is used as an observable for a rare-event process. a) Convergence of the mean value is shown for a small number of long chains starting in the C_5 region (blue), an ensemble of short chains starting in the α_L region combined with different amounts of umbrella sampling simulations (green, red, light-blue). The correct value of the C_5 to α_L transition, $\tau_{AB} = 43ns$ can be obtained already for a total simulation effort of $N = 70ns$ when short 'downhill' simulations are used in combination with umbrella sampling data. b) The standard error shows almost one order of magnitude speedup when estimating the kinetic characteristic of a rare-event τ_{AB} using short trajectories in combination with umbrella sampling simulations compared to using long trajectories and no additional information about the stationary vector.

D. Vesicle model

As a final example we consider the diffusive motion of a colloid that can reversibly attach to a surface via $m = 0, \dots, M$ tethers. A biological example of such a system is a neuronal vesicle that can attach to a plasma membrane by SNARE protein complexes. The diffusion in the solvent is free but the attachment of tethers restricts the location of the vesicle to a vicinity of the membrane. The restriction is stronger the more tethers are attached. Attachment of the vesicle to the membrane is a fast process, but the dissociation from the membrane

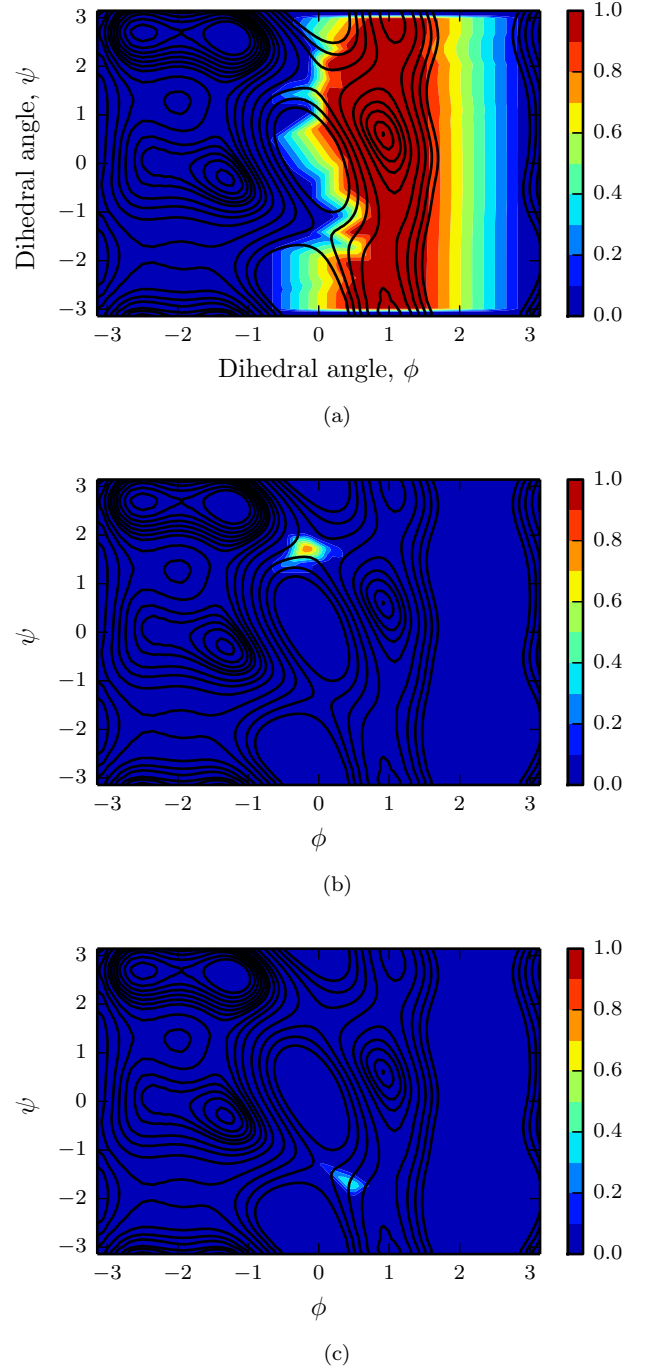


Figure 7. Forward committor $q^+(x)$ for transition from C_5 to α_L region. a) shows a non-reversible reference estimate for $N = 10\mu s$ of simulation data. Dark contour lines indicate the free energy profile. b) shows the difference between the reference estimate and a non-reversible estimate for $N = 1\mu s$ of simulation data. There is a large error in the transition region due to insufficient sampling in the short simulation. c) shows the distance for an estimate using a combination of umbrella sampling and standard simulation data with $N = N_\pi + N_C = 960ns$. There is no significant error in the transition region, the small error close to the second saddle is probably due to insufficient sampling of this region by the reference simulation.

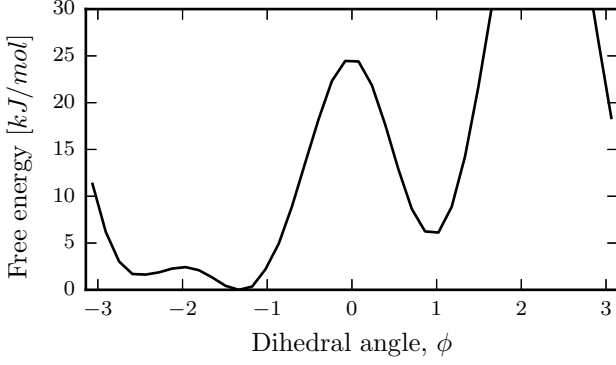


Figure 8. Free energy profile for alanine-dipeptide as a function of the ϕ dihedral angle. One can identify three meta-stable sets. Two low energy (high probability sets) with $\phi < 0$ and a single high energy (low probability) set with $\phi > 0$.

is an extremely rare event. We show that the mean first passage time for dissociation can be reliably estimated despite the fact that a non-Markovian coordinate, the membrane-vesicle distance, is used.

Figure 10 shows the energy for the different vesicle attachment modes. For $m > 0$ attachment of the vesicle to the membrane is governed by a harmonic potential close to the membrane. For $x > 2$ all attachment modes are energetically equal corresponding to a breaking of the m tethers once the distance between the vesicle and the membrane exceeds a certain threshold. The association of the vesicle has to overcome a small energetic barrier, modelling a weak repulsion of the untethered vesicle.

The state of the vesicle is given by the pair (x, m) where x is the vesicle membrane distance and m denotes the number of tethers attached. A discretization of the vesicle membrane distance with $0 = x_1 < \dots < x_d = 4$ allows us to describe the vesicle dynamics by a Markov chain on a finite state space with $(M + 1)d$ microstates. The stationary vector of the chain is given as

$$\pi = (\pi^{(0)}(x_1), \dots, \pi^{(M)}(x_d)) \quad (21)$$

with entries given in terms of the usual Gibbs/Boltzmann distribution,

$$\pi^{(m)}(x_i) \propto e^{-E^{(m)}(x_i)}. \quad (22)$$

$E^{(m)}(x)$ is the energy of a vesicle at x with m tethers attached, cf. Figure 10, (D1).

The transition matrix $P = (p_{ij})$ for the vesicle dynamics is now constructed as follows. We encode random walk probabilities in a proposal matrix $Q = (q_{ij})$. The particle moves from x_i to x_{i-1} or x_{i+1} with probability $1/3$, if the particle remains at its current position x_i it can attach, $m \rightarrow m + 1$, or detach, $m \rightarrow m - 1$, a tether with probability $1/3$ so that the overall proposal-probability for attachment or detachment is $1/9$. To account for the energetic differences of the microstates we

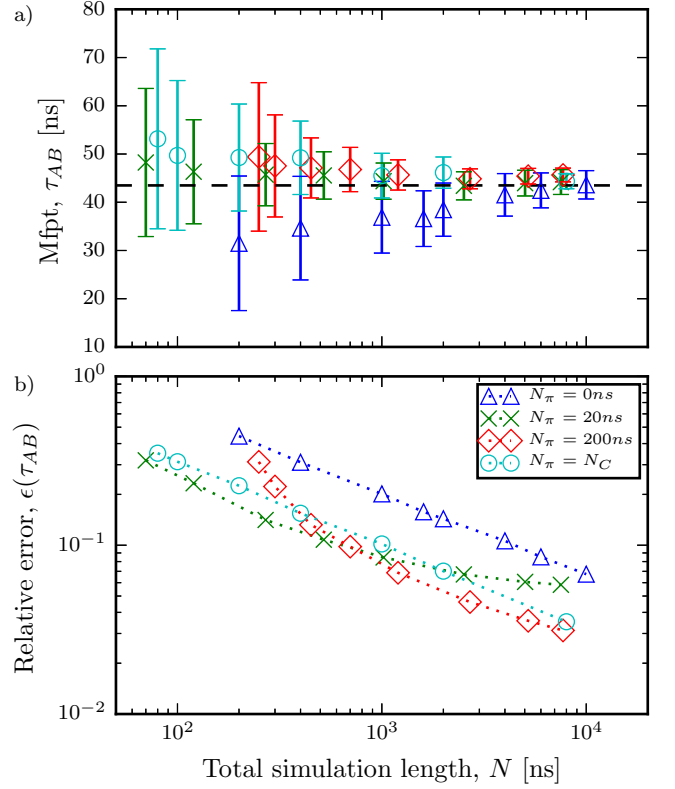


Figure 9. Mean and standard error of mean first passage time (mfpt) τ_{AB} , total simulation effort N , for alanine-dipeptide MSM on the ϕ dihedral angle alone. The mean first-passage time τ_{AB} of the transition from the low free energy region, $A = \{|\phi| - 162^\circ < \phi < -54^\circ\}$, to the high free-energy region, $B = \{\phi 36^\circ < \phi < 72^\circ\}$, is used as an observable for a rare-event process. a) Convergence of the mean value is shown for a small number of long chains starting in the A region (blue), an ensemble of short chains starting in the B region combined with different amounts of umbrella sampling simulations (green, red, light-blue). The correct value, $\tau_{AB} = 43ns$, for the C_5 to α_L transition can be obtained even if no information about the ψ dihedral angle is used in the construction of the MSM. b) The standard error shows almost one order of magnitude speedup when estimating the kinetic characteristic of a rare-event τ_{AB} using short trajectories in combination with umbrella sampling simulations compared to using long trajectories and no additional information about the stationary vector.

use the Metropolis-Hastings acceptance criterion to modulate the proposal probabilities and obtain the desired transition probabilities via,

$$p_{ij} = \min\{1, \frac{\pi_j q_{ji}}{\pi_i q_{ij}}\} \quad i \neq j. \quad (23)$$

Correct normalization is ensured by setting $p_{ii} = 1 - \sum_{j \neq i} p_{ij}$. As a result of (23) the constructed transition matrix P automatically fulfills the detailed balance condition (6) with respect to the desired stationary vector.

The mean first-passage time for the dissociation of the vesicle is $\tau_{AB} = 8.56 \cdot 10^9$, the mean first-passage time

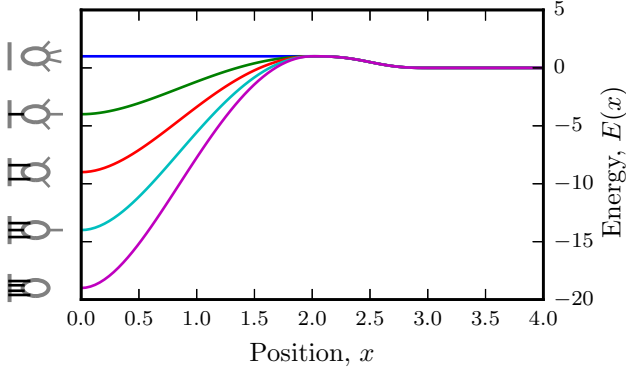


Figure 10. Energy landscape for the different attachment modes, $m = 0, 1, \dots, 4$

for association, $\tau_{BA} = 1.59 \cdot 10^3$, is orders of magnitude smaller. The mean first-passage time for dissociation of a vesicle with the maximum number of tethers attached is $\tau_{AB} = 3.83 \cdot 10^{10}$ so that the system dynamics can not be described in terms of the subspace with $m = 4$ tethers. This indicates that the dissociation kinetics is effectively non-Markovian along the x -coordinate.

The dissociation time τ_{AB} can reliably be estimated even if no information about the mode of attachment is available. If only information about the position of the vesicle is available then the state-space of the $(M+1)d$ distinct microstates is coarse-grained into d distinct sets each containing $(M+1)$ microstates corresponding to the $M+1$ possible tethering modes at position x . The coarse grained stationary vector $\tilde{\pi}$ is obtained by summing the full stationary vector π over all possible tethering modes. If short association trajectories starting in the region $x > 2$ are combined with the coarse-grained stationary vector the dissociation time can again be estimated orders of magnitude before a single dissociation event would on average be observed despite the fact that the MSM is built on a coordinate that is inherently non-Markovian. In Figure 11 we show mean and standard error for the mfpt of vesicle dissociation for a MSM build at a lagtime of $\tau = 60$ with $d = 40$ microstates.

In Figure 14 we again show convergence of the largest relaxation time and the Chapman-Kolmogorov test for an MSM constructed at lagtime $\tau = 60$. The MSM is estimated solely from short association trajectories starting in the high energy region using the coarse grained stationary vector $\tilde{\pi}$ to obtain a reversible maximum likelihood transition matrix from (9). The total simulation effort, $N = 2 \cdot 10^7$, used to obtain the MSM and perform the validation is again orders of magnitude smaller than the expected dissociation time.

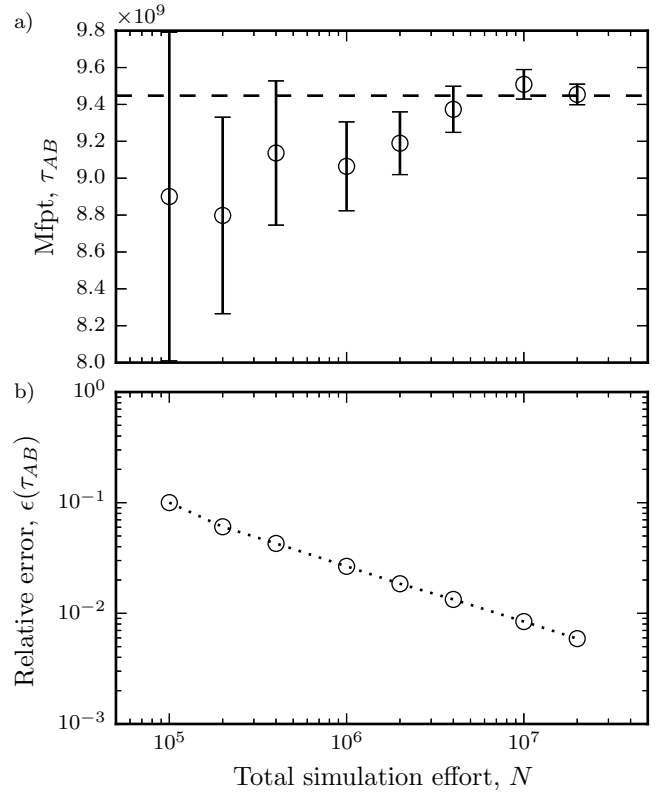


Figure 11. Mean and standard error of mean first-passage time of vesicle dissociation on a coarse-grained non-Markovian state space. a) Convergence of the mean value, b) standard error. Estimates are obtained for an ensemble of association trajectories starting in the high energy region and relaxing towards the low energy region in combination with the coarse-grained stationary probabilities. The dissociation time can be estimated orders of magnitude before a single dissociation event would have been observed.

IV. CONCLUSION

We have described a principle that allows for the first time to estimate rare-event kinetics efficiently without having to assume a simple kinetic model. Our approach is applicable when the kinetic properties of interest can be computed from a Markov state model discretization of the system. Note that this approach is qualitatively different from assuming a specific rate theory such as Transition State Theory or Kramers, because MSMs are a numerical approximation method of the full kinetics and can be made arbitrarily accurate in the limit of a good state space discretization [8] whereas a specific rate model needs to apply by design and can usually not be self-consistently validated.

The key idea of the presented approach is to use enhanced sampling methods to obtain reliable estimates of the equilibrium distribution in combination with direct simulations of the fast downhill processes. These data are combined rigorously in a reversible Markov model.

Our approach can deliver estimates of kinetic properties, including rates, passage times, but also complex quantities such as committor functions and transition path ensembles while achieving enormous speedups compared to a direct simulation.

We have illustrated our method using two toy models, a explicit-solvent MD simulation of alanine dipeptide with about 2000 degrees of freedom, and a model for reversible attachment of a vesicle to a membrane. In these examples, the kinetics of the rare events could be computed using between one and six orders of magnitude less simulation time than needed with a direct simulation approach that has to wait for the rare events to happen spontaneously.

In general, the present approach will be efficient whenever the rare-event occurs between low-probability and high-probability states. A very important example of this class is computational drug design, where the binding of the drug compound occurs relatively fast [18], while the unbinding may be many orders of magnitude slower. Yet the unbinding kinetics have been shown to be critical for drug efficacy [64].

We have demonstrated in two applications that the approach can compute kinetics from non-Markovian projections of the data: By using only the ϕ -coordinate in alanine dipeptide, and by using only the distance coordinate in the vesicle attachment model. A requirement is that the resolved coordinates are slow compared to the non-resolved coordinates. However, this requirement is not overly restrictive, as the same requirement applies for the enhanced sampling simulations, such as umbrella sampling, employed to obtain an estimate for the stationary distribution.

While the applications in the present paper have used reversible Markov model estimates in such a way that the enhanced sampling simulation and the unbiased “down-hill” simulations visit the same state space, the principle explored here can be generalized beyond this case. States visited only in one but not in the other simulation can be modelled by appropriate uninformative priors on the respective variables, e.g. uniform prior in the equilibrium distributions of states not visited in an umbrella sampling simulation.

A general framework to reconcile direct MD and enhanced MD simulations is the transition-based reweighting analysis method (TRAM) framework [29–31]. In order to apply the TRAM framework to the current setting, a hybrid TRAM method must be developed that can mix kinetic simulations (with an estimation lag time τ), and simulations that contains trajectories shorter than τ , such as those used in umbrella sampling or REMD.

The present inference principle can be exploited in an adaptive sampling framework [65, 66] to optimally distribute the computational effort between enhanced sampling and unbiased molecular dynamics simulations.

ACKNOWLEDGMENTS

We are grateful to Feliks Nüske for stimulating discussions. This work was funded by the Deutsche Forschungsgemeinschaft (DFG) grant NO825/3-1 (BTS) and a European Research Council (ERC) starting grant pcCell (FN).

Appendix A: The transition kernel for the Euler-method

The solution of (18) with initial position $X_0 = x_0$ on $[0, T]$ is usually carried out by choosing a regular discretization of the time interval

$$0 = t_0 < t_1 < \dots < t_N = T.$$

with $\Delta t = t_k - t_{k-1}$ for all $k = 1, \dots, N$. The evolution of the stochastic process is then approximated by the following time-stepping scheme

$$X_{t+\Delta t} = X_t - \nabla V(X_t)\Delta t + \sqrt{2\beta^{-1}}\eta. \quad (\text{A1})$$

with $X_0 = x_0$ and η being a $\mathcal{N}(0, \Delta t)$ distributed random variable. The time-stepping scheme (A1) is known as *Euler method* or *Euler-Maruyama method*, [67].

For this simple time-stepping scheme the transition kernel of the resulting Markov chain is given by

$$p_{\Delta t}(x, y) = \frac{1}{\sqrt{2\pi}\Delta t/2/\beta} \exp\left(-\frac{(y - x + \nabla V(x)\Delta t)^2}{2(\sqrt{\Delta t}\sqrt{2/\beta})^2}\right), \quad (\text{A2})$$

with $x = X_t$ and $y = X_{t+\Delta t}$. $p_{\Delta t}(x, y)$ is a Gaussian distribution with mean $\mu = x - \nabla V(x)\Delta t$ and variance $\sigma^2 = 2\Delta t/\beta$.

The transition probability $P_{\Delta t}(B|A)$ between two sets A, B can be computed from

$$P_{\Delta t}(B|A) = \frac{\int_A dx \pi(x) \int_B dy p_{\Delta t}(x, y)}{\int_A dx \pi(x)}. \quad (\text{A3})$$

Choosing a L such that $p_{\Delta t}(x, y)$ is effectively zero outside of $[-L, L]$ we pick a spatial discretization

$$-L = x_0 < x_1 < \dots < x_N = L \quad (\text{A4})$$

with a regular spacing $\Delta x = x_k - x_{k-1}$ for $k = 1, \dots, N$ such that $p_{\Delta t}(x, y)$ and $\pi(x)$ are approximately constant on sub-intervals $S_i = (x_i, x_{i+1}]$. In this case we have

$$\int_{x_i}^{x_{i+1}} dx \mu(x) \approx \mu(x_i)\Delta x$$

and

$$\int_{x_i}^{x_{i+1}} dx \mu(x) \int_{x_j}^{x_{j+1}} dy p(x, y) \approx \mu(x_i)p(x_i, x_j)(\Delta x)^2.$$

We can approximate the matrix elements $p_{ij} = P(S_j|S_i)$ as

$$p_{ij} \approx p(x_i, x_j) \Delta x.$$

and compute spectral properties from the matrix (p_{ij}) using standard eigenvalue solvers.

Appendix B: Mean first-passage times between meta-stable regions

The covered material can be found in many introductory books to stochastic processes, cf. [68].

For a stochastic process (X_t) on a state space Ω the first hitting time T_B of a set $B \subseteq \Omega$ is defined as

$$T_B = \inf\{t \geq 0 | X_t \in B\}. \quad (\text{B1})$$

The mean first passage time $\tau_{x,B}$ to the set B starting in state $x \in \Omega$ is the following expectation value

$$\tau_{x,B} = \mathbb{E}_x(T_B). \quad (\text{B2})$$

For a Markov chain on a finite state space $\Omega = \{1, \dots, n\}$ with transition matrix $(p_{x,y})$ the mean first-passage time can be computed from the following system of equations,

$$\tau_{x,B} = \begin{cases} 0 & x \in B \\ 1 + \sum_{y \in \Omega} p_{x,y} \tau_{y,B} & x \notin B \end{cases} \quad (\text{B3})$$

Assuming that the chain has stationary vector (μ_x) we define the mean first-passage time $\tau_{A,B}$ from set A to

set B as the μ -weighted average of all mean first-passage times to B when starting in a state $x \in A$,

$$\tau_{A,B} = \sum_{x \in A} \mu_x \tau_{x,B}. \quad (\text{B4})$$

Computing the mean first-passage time between two sets for a Markov chain on a finite state space with given transition matrix thus amounts to finding the stationary vector together with the solution of a linear system of equations - both of which can be achieved using standard numerical linear algebra libraries.

Appendix C: Committor functions

Committor functions have been introduced in the context of Transition Path Theory [12] and are a central object for the characterisation of transition processes between two meta-stable sets.

Let (X_t) again be a stochastic process on a state space Ω and let $A, B \subseteq \Omega$ be two meta-stable sets. The forward committor $q^{(+)}(x)$ is the probability that the process starting in x will reach the set B first, rather than the set A ,

$$q^{(+)}(x) = \mathbb{P}_x(T_A < T_B). \quad (\text{C1})$$

Again T_S denotes the first hitting time of a set S .

For a Markov chain on a finite state space with transition matrix P the forward committor solves the following boundary value problem [13],

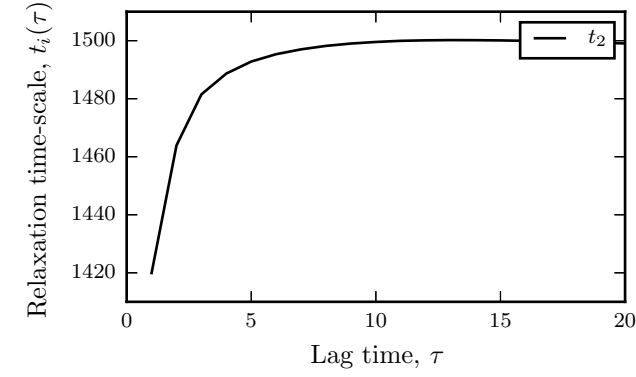
$$\begin{aligned} \sum_j l_{ij} q_j^{(+)} &= 0 & i \in X \setminus (A \cup B) \\ q_i^{(+)} &= 0 & i \in A \\ q_i^{(+)} &= 1 & i \in B \end{aligned} \quad (\text{C2})$$

$L = P - I$ is the corresponding generator matrix of the Markov chain.

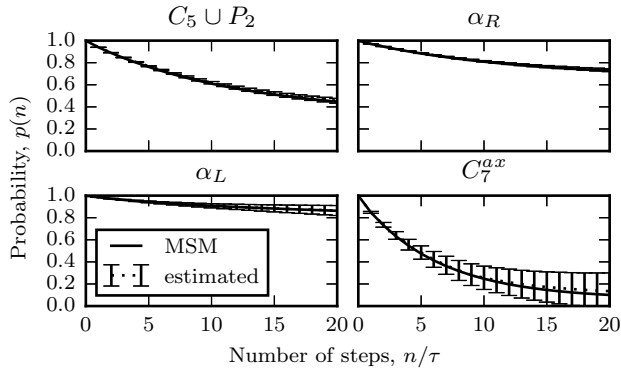
Computing the committor for a finite state space again amounts to solving a linear system of equations.

Appendix D: Vesicle potential

$$E^{(m)}(x) = \begin{cases} 1 + m(-5 + 5x^2 - 2.5x^3 + 0.3125x^4) & 0 \leq x < 2 \\ 1 + 8(x-2)^2 - 8(x-2)^3 & 2 \leq x < 2.5 \\ 0.5 - 8(x-2.5)^2 + 8(x-2.5)^3 & 2.5 \leq x < 3 \\ 0 & 3 \leq x < 4 \end{cases} \quad (\text{D1})$$



(a)



(b)

Figure 12. a) Implied timescale test. Convergence of the largest relaxation time-scale, t_2 , indicates a good Markov model fit, i.e. the slow eigenfunction of the associated dynamical operator are well approximated. b) The Chapman-Kolmogorov test validates the Markov assumption by comparing the evolution of self-transition probabilities predicted by the MSM parametrized at lagtime τ with direct estimates from the data at larger lagtimes $n\tau$.

Appendix E: MSM validation

-
- | | |
|---|--|
| <p>[1] C. Schütte, A. Fischer, W. Huisinga, and P. Deuffhard, J. Comp. Phys. 151, 146 (1999).</p> <p>[2] W. C. Swope, J. W. Pitera, and F. Suits, J. Phys. Chem. B 108, 6571 (2004).</p> <p>[3] N. Singhal, C. D. Snow, and V. S. Pande, J. Chem. Phys. 121, 415 (2004).</p> <p>[4] J. D. Chodera, K. A. Dill, N. Singhal, V. S. Pande, W. C. Swope, and J. W. Pitera, J. Chem. Phys. 126, 155101 (2007).</p> <p>[5] F. Noé, I. Horenko, C. Schütte, and J. C. Smith, J. Chem. Phys. 126, 155102 (2007).</p> | <p>[6] A. Pan and B. Roux, J. Chem. Phys. 129 (2008).</p> <p>[7] N. V. Buchete and G. Hummer, J. Phys. Chem. B 112, 6057 (2008).</p> <p>[8] J.-H. Prinz, H. Wu, M. Sarich, B. Keller, M. Senne, M. Held, J. D. Chodera, C. Schütte, and F. Noé, J. Chem. Phys. 134, 174105 (2011).</p> <p>[9] M. Senne, B. Trendelkamp-Schroer, A. S. Mey, C. Schütte, and F. Noé, J. Chem. Theory Comput. 8, 2223 (2012).</p> <p>[10] K. A. Beauchamp, G. R. Bowman, T. J. Lane, L. Maibaum, I. S. Haque, and V. S. Pande, J. Chem.</p> |
|---|--|

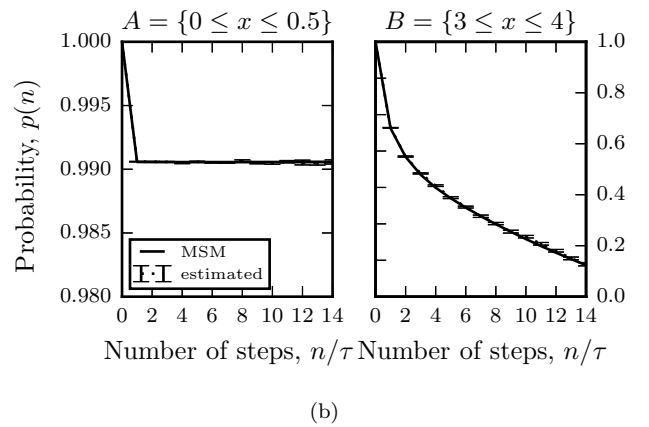
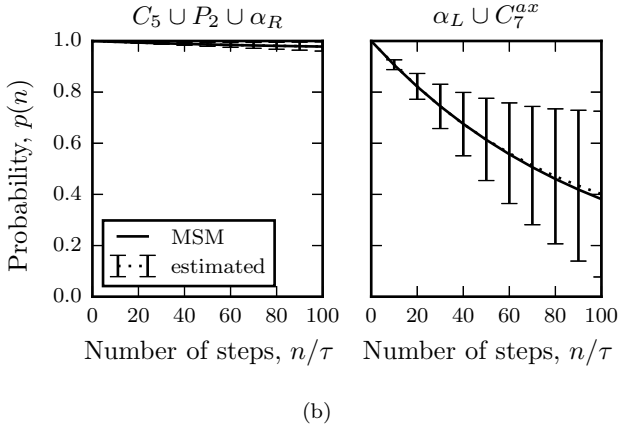
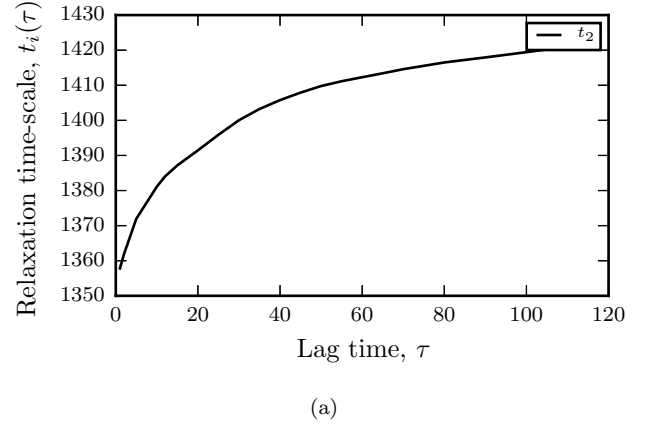
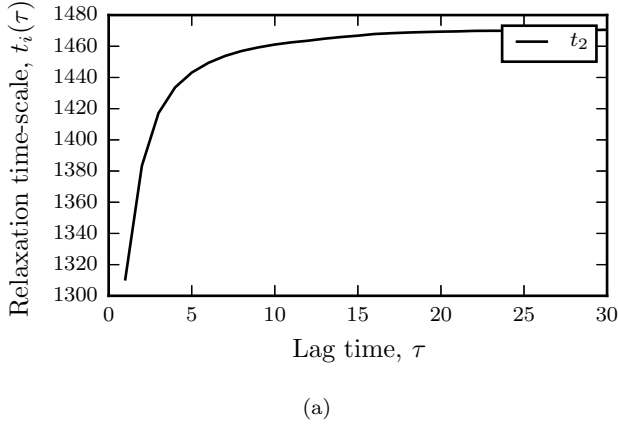


Figure 13. a) Implied timescale test. Convergence of the largest relaxation time-scale, t_2 , indicates a good Markov model fit, i.e. the slow eigenfunction of the associated dynamical operator are well approximated. b) The Chapman-Kolmogorov test validates the Markov assumption by comparing the evolution of self-transition probabilities predicted by the MSM parametrized at lagtime τ with direct estimates from the data at larger lagtimes $n\tau$.

Figure 14. a) Implied timescale test. Convergence of the largest relaxation time-scale, t_2 , indicates a good Markov model fit, i.e. the slow eigenfunction of the associated dynamical operator are well approximated. b) The Chapman-Kolmogorov test validates the Markov assumption by comparing the evolution of self-transition probabilities predicted by the MSM parametrized at lagtime τ with direct estimates from the data at larger lagtimes $n\tau$. Values were obtained from an ensemble of short trajectories starting in the high energy region utilizing the stationary vector in the estimation of the MLE transition matrix, cf. (9).

Theory Comput. **7**, 3412 (2011).

- [11] M. Sarich, F. Noé, and C. Schütte, Multiscale Model. Simul. **8**, 1154 (2010).
- [12] W. E and E. Vanden-Eijnden, J. Stat. Phys. **123**, 503 (2006).
- [13] P. Metzner, C. Schütte, and E. Vanden-Eijnden, Multiscale Model. Simul. **7**, 1192 (2009).
- [14] F. Noé, C. Schütte, E. Vanden-Eijnden, L. Reich, and T. R. Weikl, Proc. Natl. Acad. Sci. USA **106**, 19011 (2009).
- [15] V. A. Voelz, G. R. Bowman, K. A. Beauchamp, and V. S. Pande, J. Am. Chem. Soc. **132**, 1526 (2010).
- [16] M. Held, P. Metzner, J.-H. Prinz, and F. Noé, Biophys. J. **100**, 701 (2011).
- [17] S. Gu, D.-A. Silva, L. Meng, A. Yue, and X. Huang, PLoS Comput. Biol. **10**, e1003767 (2014).
- [18] I. Buch, T. Giorgino, and G. de Fabritiis, Proc. Natl. Acad. Sci. USA **108**, 10184 (2011).
- [19] D. E. Shaw, P. Maragakis, K. Lindorff-Larsen, S. Piana, R. O. Dror, M. P. Eastwood, J. A. Bank, J. M. Jumper,

- J. K. Salmon, Y. Shan, *et al.*, Science **330**, 341 (2010).
- [20] G. Torrie and J. Valleau, J. Comp. Phys. **23**, 187 (1977).
- [21] H. Grubmüller, Phys. Rev. E **52**, 2893 (1995).
- [22] Y. Sugita and Y. Okamoto, Chem. Phys. Lett. **314**, 141 (1999).
- [23] A. Laio and M. Parrinello, Proc. Natl. Acad. Sci. USA **99**, 12562 (2002).
- [24] H. Eyring, J. Chem. Phys. **3**, 107 (1935).
- [25] H. Kramers, Physica **7**, 284 (1940).
- [26] R. B. Best and G. Hummer, Proc. Natl. Acad. Sci. USA **107**, 1088 (2010).
- [27] P. Tiwary and M. Parrinello, Phys. Rev. Lett. **111**, 230602 (2013).
- [28] E. Rosta and G. Hummer, Journal of Chemical Theory and Computation **11**, 276 (2015).
- [29] H. Wu and F. Noé, Multiscale Modeling & Simulation **12**, 25 (2014).

- [30] H. Wu, A. Mey, E. Rosta, and F. Noé, *The Journal of Chemical Physics* **141**, 214106 (2014).
- [31] A. Mey, H. Wu, and F. Noé, *Phys. Rev. X* **4**, 041018 (2014).
- [32] P. G. Bolhuis, D. Chandler, C. Dellago, and P. L. Geissler, *Annu. Rev. Phys. Chem.* **53**, 291 (2002).
- [33] A. K. Faradjian and R. Elber, *J. Chem. Phys.* **120**, 10880 (2004).
- [34] T. S. van Erp, D. Moroni, and P. G. Bolhuis, *J. Chem. Phys.* **118** (2003).
- [35] W.-N. Du and P. G. Bolhuis, *J. Chem. Phys.* **139**, 044105 (2013).
- [36] W. F. Van Gunsteren and H. J. C. Berendsen, *Mol. Simulat.* **1**, 173 (1988).
- [37] M. Tuckerman, B. J. Berne, and G. J. Martyna, *J. Chem. Phys.* **97**, 1990 (1992).
- [38] S. Sriraman, I. G. Kevrekidis, and G. Hummer, *J. Phys. Chem. B* **109**, 6479 (2005).
- [39] F. Noé, *J. Chem. Phys.* **128**, 244103 (2008).
- [40] K. Wang, J. D. Chodera, Y. Yang, and M. R. Shirts, *J. Comput. Aided Mol. Des.* **27**, 989 (2013).
- [41] M. Souaille and B. Roux, *Comput. Phys. Commun.* **135**, 40 (2001).
- [42] R. Zwanzig, *J. Stat. Phys.* **9**, 215 (1973).
- [43] C. W. Gardiner, *Applied Optics* **25**, 3145 (1986).
- [44] C. Schütte, “Conformational dynamics: Modeling, theory, algorithm, and application to biomolecules,” (1999), habilitation thesis.
- [45] C. Schütte and W. Huisinga, “On conformational dynamics induced by langevin processes,” in *Equadiff 99* (2000) Chap. 234, pp. 1247–1262.
- [46] F. Wang and D. P. Landau, *Phys. Rev. Lett.* **86**, 2050 (2001).
- [47] S. Trebst and M. Troyer, in *Computer Simulations in Condensed Matter: From Materials to Chemical Biology. Volume 1*, edited by M. Ferrario, G. Ciccotti, and K. Binder (Springer, 2006).
- [48] C. H. Bennett, **22**, 245 (1976).
- [49] A. M. Ferrenberg and R. H. Swendsen, *Physical Review Letters* **63**, 1195 (1989).
- [50] S. Kumar, J. Rosenberg, D. Bouzida, R. Swendsen, and P. Kollman, *J. Comp. Chem.* **16**, 1339 (1995).
- [51] Z. Tan, *J. Amer. Statist. Assoc.* **99**, 1027 (2004).
- [52] M. R. Shirts and J. D. Chodera, *J. Chem. Phys.* **129**, 124105 (2008).
- [53] B. Trendelkamp-Schroer, H. Wu, F. Paul, and F. Noé, *J. Chem. Phys.* (2015, submitted).
- [54] S. Kumar, J. M. Rosenberg, D. Bouzida, R. H. Swendsen, and P. A. Kollman, *J. Comput. Chem.* **13**, 1011 (1992).
- [55] B. Efron and R. J. Tibshirani, *An introduction to the bootstrap* (CRC press, 1994).
- [56] B. Montgomery Pettitt and M. Karplus, *Chem. Phys. Lett.* **121**, 194 (1985).
- [57] A. G. Anderson and J. Hermans, *Proteins* **3**, 262 (1988).
- [58] D. J. Tobias and C. L. Brooks III, *J. Phys. Chem.* **96**, 3864 (1992).
- [59] J. D. Chodera, W. C. Swope, J. W. Pitera, and K. A. Dill, *Multiscale Model. Simul.* **5**, 1214 (2006).
- [60] W.-N. Du, K. A. Marino, and P. G. Bolhuis, *J. Chem. Phys.* **135**, 145102 (2011).
- [61] P. Eastman, M. S. Friedrichs, J. D. Chodera, R. J. Radmer, C. M. Bruns, J. P. Ku, K. A. Beauchamp, T. J. Lane, L.-P. Wang, D. Shukla, T. Tye, M. Houston, T. Stich, C. Klein, M. R. Shirts, and V. S. Pande, *J. Chem. Theory Comput.* **9**, 461 (2013).
- [62] K. Lindorff-Larsen, S. Piana, K. Palmo, P. Maragakis, J. L. Klepeis, R. O. Dror, and D. E. Shaw, *Proteins* **78**, 1950 (2010).
- [63] W. L. Jorgensen, J. Chandrasekhar, J. D. Madura, R. W. Impey, and M. L. Klein, *J. Chem. Phys.* **79**, 926 (1983).
- [64] P. J. Tummino and R. A. Copeland, *Biochemistry* **47**, 5481 (2008).
- [65] G. R. Bowman, D. L. Ensign, and V. S. Pande, *J. Chem. Theory Comput.* **6**, 787 (2010).
- [66] S. Doerr and G. De Fabritiis, *J. Chem. Theory Comput.* **10**, 2064 (2014).
- [67] P. E. Kloeden and E. Platen, *Numerical solution of stochastic differential equations*, Vol. 23 (Springer, 1992).
- [68] P. G. Hoel, S. C. Port, and C. J. Stone, *Introduction to stochastic processes* (Waveland Press, 1986).